coatings

Communication

Improving the Electrochemical Performance of $LiNi_{1/3}Co_{1/3}Mn_{1/3}O_2$ Cathode Material by LiF Modification

Sisi Zhou [1], Xianggong Zhang [1], Zhihao Zhang [2], Songting Liu [2,*] and Rui Wang [2,*]

1 Wuhan Institute of Marine Electric Propulsion, Wuhan 430064, China
2 Faculty of Materials Science and Chemistry, China University of Geosciences, Wuhan 430074, China
* Correspondence: 1202120176@cug.edu.cn (S.L.); wangrui@cug.edu.cn (R.W.)

Abstract: $LiNi_{1/3}Co_{1/3}Mn_{1/3}O_2$ is a widely used commercial cathode material in the fields of consumer electronics and electric vehicles. However, its energy density still falls short of the standard and needs to be improved. The most effective method is to increase the cut-off voltage, but this will result in a drop in capacity. In this study, a LiF layer is coated on the surface of $LiNi_{1/3}Co_{1/3}Mn_{1/3}O_2$ via an in situ method. It is found that the LiF layer may protect materials from side reactions with electrolytes, improve the interfacial stability, and enhance the cyclic performance. The bare sample shows relatively poor cycling stability, with capacity retention rates of 65.9% (0.2 C) and 12.8% (5 C) after 100 cycles, while 1% LiF-coated NCM has higher cycling stability with capacity retention rates of 83.4% (0.2 C) and 73.3% (5 C) after 100 cycles, respectively. Our findings suggest that a LiF surface layer could be a useful means of boosting the electrochemical performance of NCM cathode materials.

Keywords: lithium-ion batteries; cathode; $LiNi_{1/3}Co_{1/3}Mn_{1/3}O_2$; surface modification

check for updates

Citation: Zhou, S.; Zhang, X.; Zhang, Z.; Liu, S.; Wang, R. Improving the Electrochemical Performance of $LiNi_{1/3}Co_{1/3}Mn_{1/3}O_2$ Cathode Material by LiF Modification. *Coatings* **2023**, *13*, 727. https://doi.org/10.3390/coatings13040727

Academic Editors: Stanica Enache, Konstantin Petrov and Mirela Dragan

Received: 16 February 2023
Revised: 7 March 2023
Accepted: 14 March 2023
Published: 3 April 2023

1. Introduction

Lithium-ion batteries are widely utilized in various consumer electronics due to their exceptional performance. However, the growing demand for high energy density and high-capacity batteries in electric vehicles and renewable energy storage has increased the demand for better lithium-ion batteries (LIBs) [1–6]. One of the most promising cathode materials for LIBs is the layered transition metal oxide $LiNi_xCo_yMn_{1-x-y}O_2$, which offers benefits such as low cost, high specific capacity, good cycling stability, and thermal stability [7–9]. $LiNi_{1/3}Co_{1/3}Mn_{1/3}O_2$ (NCM), one variant of this cathode material, has garnered attention due to its potential for research and application [10,11]. However, it has limitations such as low tap density, low initial coulombic efficiency, rapid capacity decay, and poor rate performance under high cut-off voltage [12,13].

To address these limitations, various surface-modified materials have been employed to protect the active materials and improve their cycling performance. Reported surface materials can be classified into two different kinds. Firstly, fluorides (AlF_3, CaF_2, CoF_2) [14–16], oxides (TiO_2, Al_2O_3) [17,18], and phosphates (Li_3PO_4, $AlPO_4$, $FePO_4$) [19–21] can inhibit side reactions between the electrode and electrolyte and improve the cycling stability. Secondly, fast ionic conductors such as $Li_{1.3}Al_{0.3}Ti_{1.7}(PO_4)_3$ [22] can accelerate the Li^+ diffusion and improve the rate performance.

LiF is a critical component of both cathode electrolyte interphase (CEI) and solid electrolyte interphase (SEI) [23–25]. It has been reported to be as an effective surface layer to improve the electrochemical performances of Li-excess materials [26,27]. Studies suggest that it is crucial in facilitating Li^+ transfer and preserving the stability of the electrode/electrolyte interface, without adding extra metal ions to the cathode [28–30]. NCM shares a similar layered structure with Li-excess materials. In this case, whether the effectiveness of its role in Li-excess materials is still effective in NCM deserves to be studied. In this research, a thin and uniform LiF surface layer was in situ formed on NCM particles through the thermal decomposition of $LiPF_6$. The resulting LiF-coated NCM showed significant improvements in cycling stability and rate performance at high cut-off voltage.

2. Experimental

2.1. Sample Preparation

The NCM cathode material was purchased from the Cyber Electrochemical Materials Network. LiF-Coated NCM was synthesized as follows. Firstly, NCM, $LiPF_6$ and anhydrous ethanol were blended under continuous stirring for 24 h at 25 °C. Secondly, the liquid mixture was dried in an air-circulating oven at 80 °C for 12 h. Then, the solid mixture was calcined in a muffle furnace (Beiyike, Hefei, China) at 350 °C for 2 h under a controlled atmosphere to decompose $LiPF_6$ into LiF. The mass ratio of NCM to $LiPF_6$ was varied as 1:0, 1:0.005, 1:0.01, and 1:0.02, resulting in the respective products labeled as 0%LiF@NCM, 0.5%LiF@NCM, 1%LiF@NCM, and 2%LiF@NCM, respectively. The detailed synthesizing process of the modified NCM is illustrated in Figure 1.

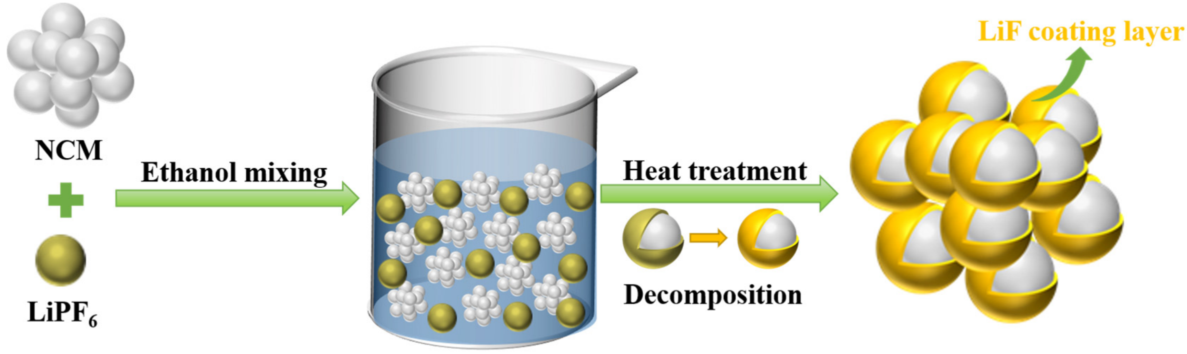

Figure 1. Schematic diagram of the decomposition of $LiPF_6$ and the formation of LiF on NCM particles.

2.2. Characterization of Materials

The crystal structures of as-prepared materials were analyzed by X-ray diffraction (XRD; Cu Kα radiation, λ = 1.5406 Å, Bruker D8-FOCUS, Bruker, Karlsruhe, Germany). The morphologies and structures of samples were observed using a scanning electron microscope (SEM; SU3500, Hitachi, Tokyo, Japan) and a high-resolution transmission electron microscope (HRTEM; Tecnai G2 F20 S-TWIN TMP, FEI, Eindhoven, Netherland). The element distributions were characterized by an energy-dispersive X-ray spectrometer (EDS, SU8010, Hitachi, Tokyo, Japan). The valence states of elements were determined by X-ray photoelectron spectroscopy (XPS, ESCALab 250Xi, Thermo Scientific, Waltham, MA, USA).

2.3. Electrochemical Characterization

To make an electrode, LiF@NCM, Super P, and polyvinylidene fluoride (PVDF) were weighed and mixed at a mass ratio of 8:1:1 with N-methylpyrrolidone (NMP). Then, the slurry was evenly coated on aluminum foil and dried in an air-circulating oven at 80 °C for 24 h. Coin cells were assembled using lithium metal as the counter electrode, a glass fiber as the separator, and 1 M $LiPF_6$ solution (EC:DMC = 1:1, v/v) as the electrolyte in an Ar-filled glove box. Galvanostatic charge-discharge and rate tests were conducted using a battery testing system (LANHE CT2001A, Land, Wuhan, China) at room temperature with a voltage range of 2.5 to 4.6 V (1C = 200 mAh g^{-1}). Cyclic voltammetry was performed on an electrochemical station (Chenhua, Shanghai, China) with a scan rate of 0.3 mV s^{-1} in a voltage range of 2.5 to 4.6 V. Electrochemical impedance spectroscopy was recorded in a frequency range from 0.01 Hz to 1 MHz.

3. Results and Discussion

Figure 2 displays XRD patterns LiF and the LiF-coated NCM samples. The main diffraction peaks of the LiF-coated NCM samples all correspond to the typical α-$NaFeO_2$ structure (space group: R-3m) [31], which indicates that the structure of NCM remains unchanged after the LiF coating. Based on the XRD results, no diffraction peaks of LiF were detected.

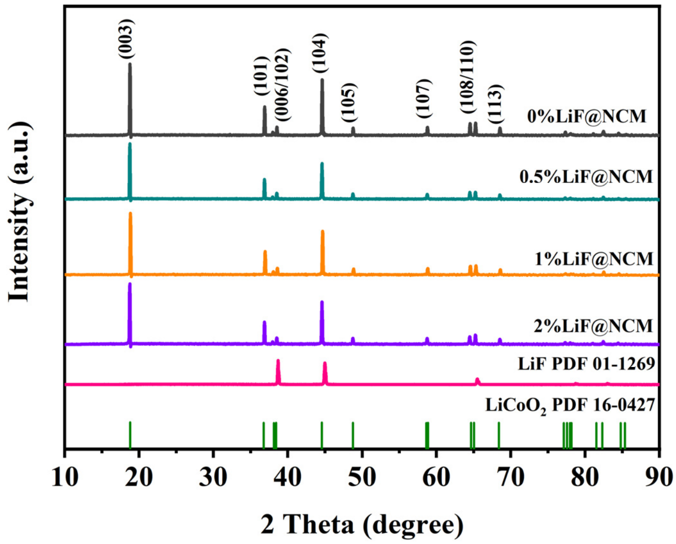

Figure 2. XRD patterns of 0%LiF@NCM, 0.5%LiF@NCM, 1%LiF@NCM, 2%LiF@NCM and LiF.

Figure 3 depicts SEM images of the four samples. The commercial NCM is a large, smooth particle of approximately 5–10 μm, consisting of primary particles of different sizes (Figure 3a). The LiF-modified NCM samples show similar morphology to the bare one, indicating that surface modification of LiF does not significantly change the surface structure of NCM (Figure 3b–d). Elemental mapping experiments were conducted to analyze the elemental compositions of the LiF-coated samples. As shown in Figure 4, Mn, Co, Ni, and F elements are uniformly distributed in 0.5%LiF@NCM, 1%LiF@NCM, and 2%LiF@NCM. The absence of a noticeable signal of the P element suggests that $LiPF_6$ was decomposed into LiF during heat treatment, and LiF is uniformly distributed on the surface of NCM according to the F signal.

HRTEM was used to directly observe the surface layer on NCM. For the 0%LiF@NCM sample (Figure 5a), clear lattice fringe can be observed up to the edge. The interplanar distance was calculated to be 0.47 nm, which should be related to the (003) crystal face of the layered structure [32]. For the 1%LiF@NCM sample, nanoparticles with an interplanar distance of 0.23 nm can be distinguished, corresponding to the (111) crystal plane of LiF [33]. This result directly confirms the presence of a LiF layer on the surface of NCM.

The XPS spectra of the 0%LiF@NCM and 1%LiF@NCM samples are shown in Figure 6. For 0%LiF@NCM, characteristic peaks of C, O, Ni, Mn, and Co can be clearly observed. For the 1%LiF@NCM sample, a characteristic peak of F at 685.0 eV is observed, while the peak of P is not detected. Figure 6c–e show the high-resolution XPS spectra of the Ni, Mn, and Co elements. The Ni 2p spectra of both samples (Figure 6c) show two peaks at 854.9 eV ($2p_{3/2}$) and 872.2 eV ($2p_{1/2}$), which can both be identified as Ni^{2+} [34]. In the Mn spectra shown in Figure 6d, two peaks at 642.8 eV and 641. 8 eV can be ascribed to Mn^{4+} and Mn^{3+}, respectively. [35]. In Figure 6e, the two peaks at 780.1 eV and 795.3 eV can be identified as Co^{3+} [36]. The positions of the peaks of Ni, Mn, Co are nearly the same in the two samples, which infers the valences of the three elements remains unchanged after the surface treatment.

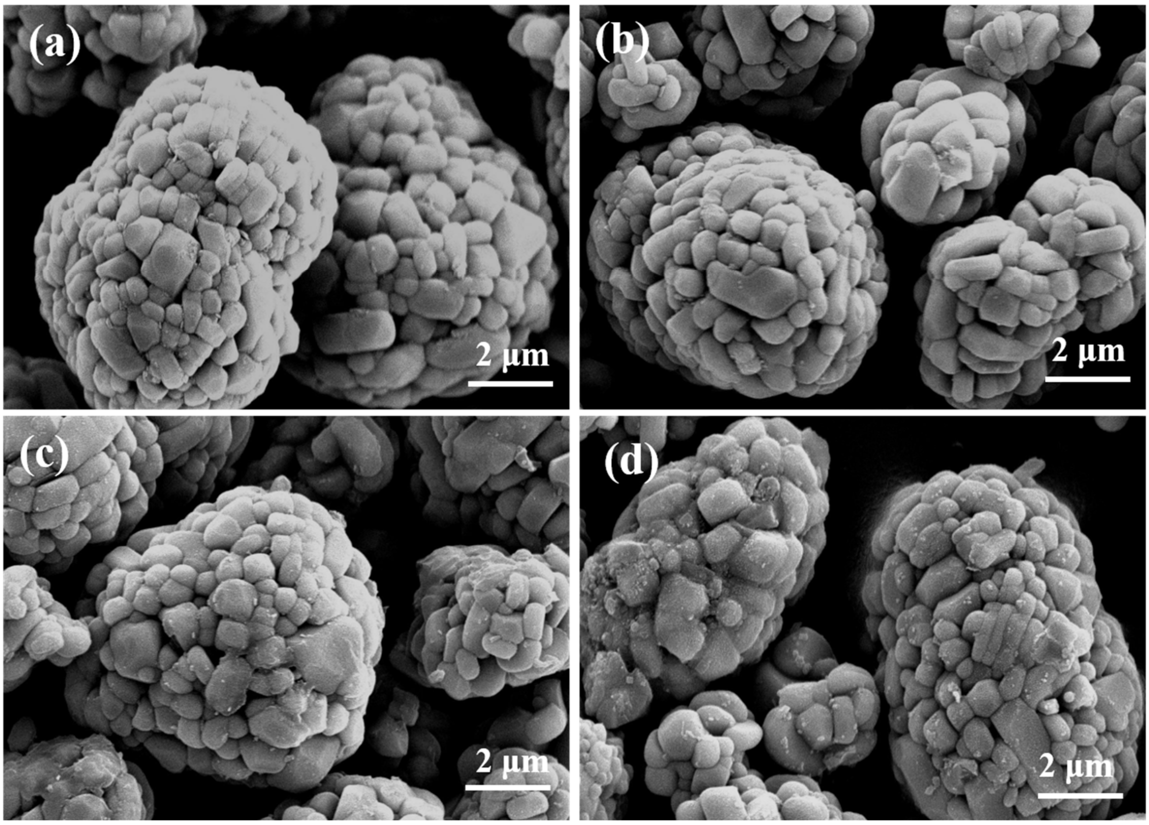

Figure 3. SEM images of (**a**) 0%LiF@NCM, (**b**) 0.5%LiF@NCM, (**c**) 1%LiF@NCM, and (**d**) 2%LiF@NCM.

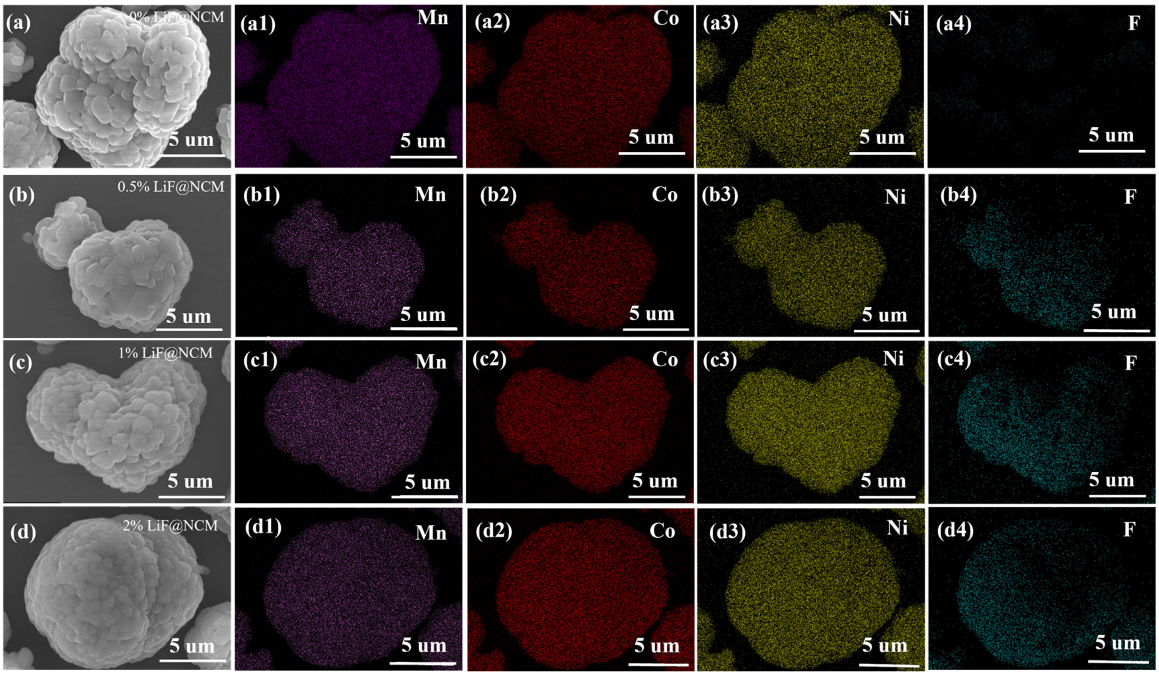

Figure 4. Elemental mapping images of (**a**) 0%LiF@NCM((**a1**) Mn, (**a2**) Co, (**a3**) Ni, (**a4**) F), (**b**) 0.5%LiF@NCM ((**b1**) Mn, (**b2**) Co, (**b3**) Ni, (**b4**) F), (**c**) 1%LiF@NCM ((**c1**) Mn, (**c2**) Co, (**c3**) Ni, (**c4**) F), and (**d**) 2%LiF@NCM ((**d1**) Mn, (**d2**) Co, (**d3**) Ni, (**d4**) F).

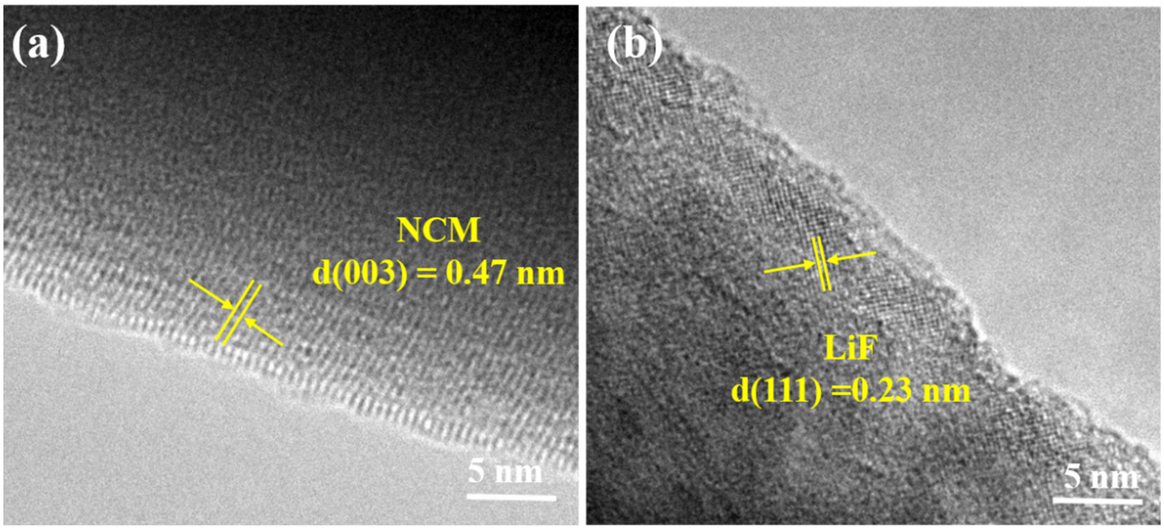

Figure 5. HRTEM images of (**a**) 0%LiF@NCM and (**b**) 1%LiF@NCM.

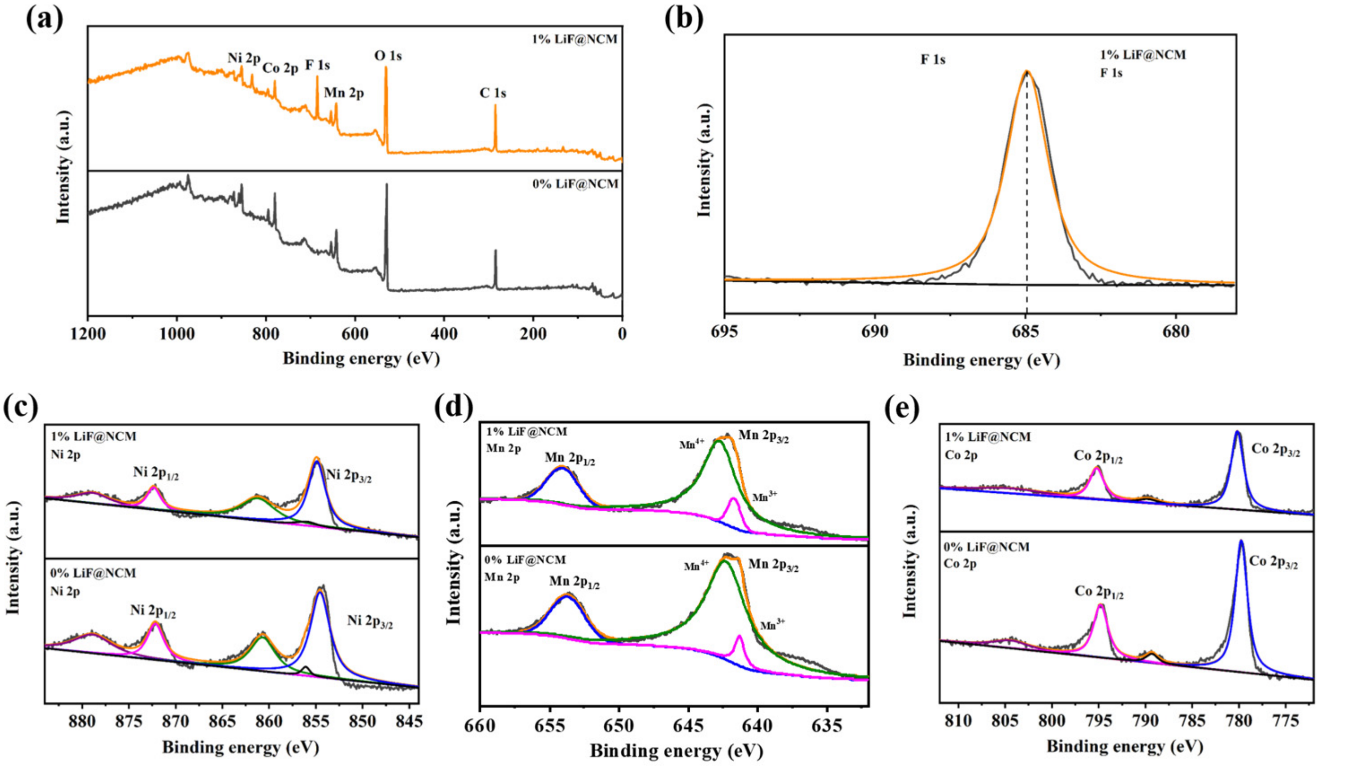

Figure 6. (**a**) XPS survey spectra of 0%LiF@NCM and 1%LiF@NCM; (**b**) F 1s XPS spectra of 1%LiF@NCM; (**c**) Ni 2p XPS spectra of 0%LiF@NCM and 1%LiF@NCM; (**d**) Mn 2p XPS spectra of 0%LiF@NCM and 1%LiF@NCM; (**e**) Co 2p XPS spectra of 0%LiF@NCM and 1%LiF@NCM.

The charge-discharge profiles of all samples in the first cycle are shown in Figure 7a. The initial discharge capacity of commercial NCM is 176.7 mAh g^{-1}. After the LiF treatment, the initial discharge capacities of the three samples are all slightly larger than the untreated one. Additionally, for the 2%LiF@NCM sample, clear polarization can be observed in the initial charge. The reason may be the LiF surface is too thick, which hinders the transport of lithium ions. Figure 7b demonstrates the rate capabilities of the four samples at rates from 0.2C to 5C. The three modified NCM samples all show improved rate performances compared to the bare sample. Among them, the 1%LiF@NCM sample exhibits the best performance. Specifically, when the rate is 5C, the discharge capacities of the bare NCM and 1%LiF@NCM samples are 99.5 mAh g^{-1} and 142.9 mAh g^{-1}, respectively, representing a 44% improvement for the latter one. The cycling performances of all samples at 0.2C and 2C are shown in Figure 7c,d. The bare sample exhibits relatively poor cycling stability, with capacity retentions of 65.9% (0.2 C) and 12.8% (5 C) after 100 cycles. However, 1%LiF@NCM exhibits much-improved cycling stability, with capacity retentions of 83.4% (0.2 C) and 73.3% (5 C) after 100 cycles, respectively. In conclusion, the in-situ-formed LiF surface layer can significantly improve the rate and cycling performances of NCM.

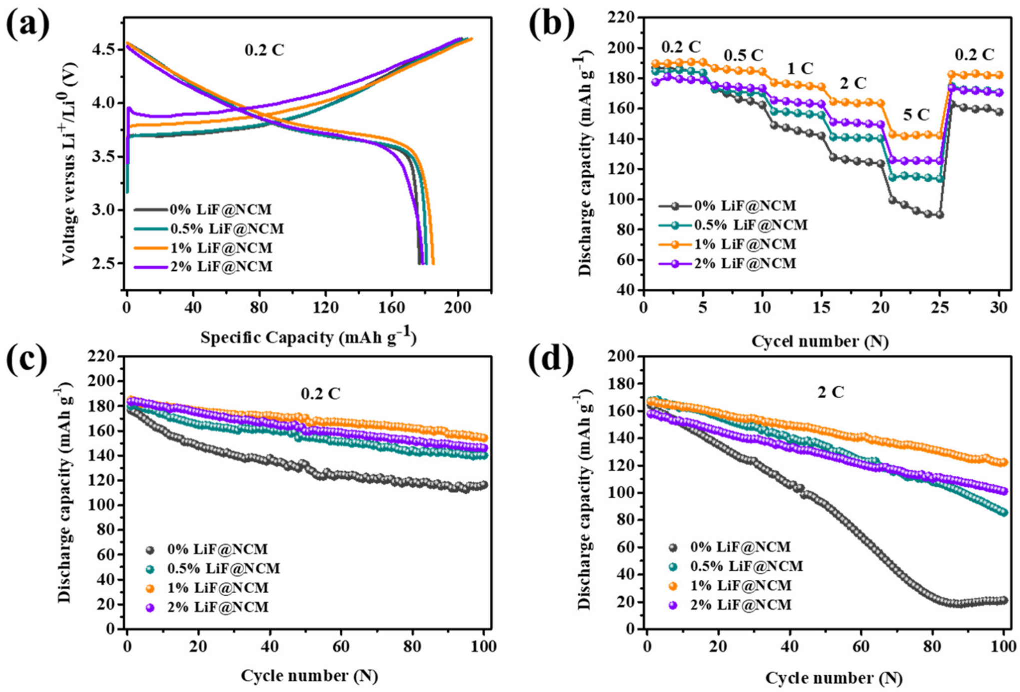

Figure 7. The electrochemical properties of 0%LiF@NCM, 0.5%LiF@NCM, 1%LiF@NCM, and 2%LiF@NCM: (**a**) the initial charge-discharge curves at 0.2C; (**b**) rate performance from 0.2C to 5C; (**c**) cycling performances at 0.2C; (**d**) cycling performances at 2 C.

A more detailed comparison of the electrochemical performances of the 0% and 1%LiF@NCM samples is shown in Figure 8a,b. It can be seen that the discharge capacities of the untreated sample drop rapidly, while for the 1%LiF@NCM sample, it still could deliver a capacity higher than 120 mAh g^{-1} after 100 cycles. The dQ/dV curves of the two samples are presented in Figure 8c,d. The dQ/dV curves of the two samples are presented in Figure 8c,d. For the untreated sample, during the cycles, a broad voltage peak below 3 V appears, which is characteristic of the spinel phase. The reason for this phase transition is due to the instability at the interface. This phase transition is irreversible and would lead to a decrease in both capacity and voltage [37]. Conversely, this phase transition is suppressed in the 1% LiF@NCM sample. As shown in Figure 8d, the cathodic peak is still around 3.5 V after 100 cycles, which indicates this material exhibits better stability during cycling.

To better understand the effects of a LiF layer on the improvements of electrochemical performances, EIS measurements were conducted on the bare NCM and 1%LiF@NCM samples. As shown in Figure 9, the Nyquist curves consist of a semicircle at the mid-high frequency region and a quasi-straight line in the low frequency region [38,39]. It is clear that the curves of the two samples after the 1st cycle are similar. However, after 5 and 50 cycles, the semicircles of 1%LiF@NCM are significantly smaller than those of 0%LiF@NCM, which indicates the surface of 1%LiF@NCM is more stable and the ion transport is much faster [40].

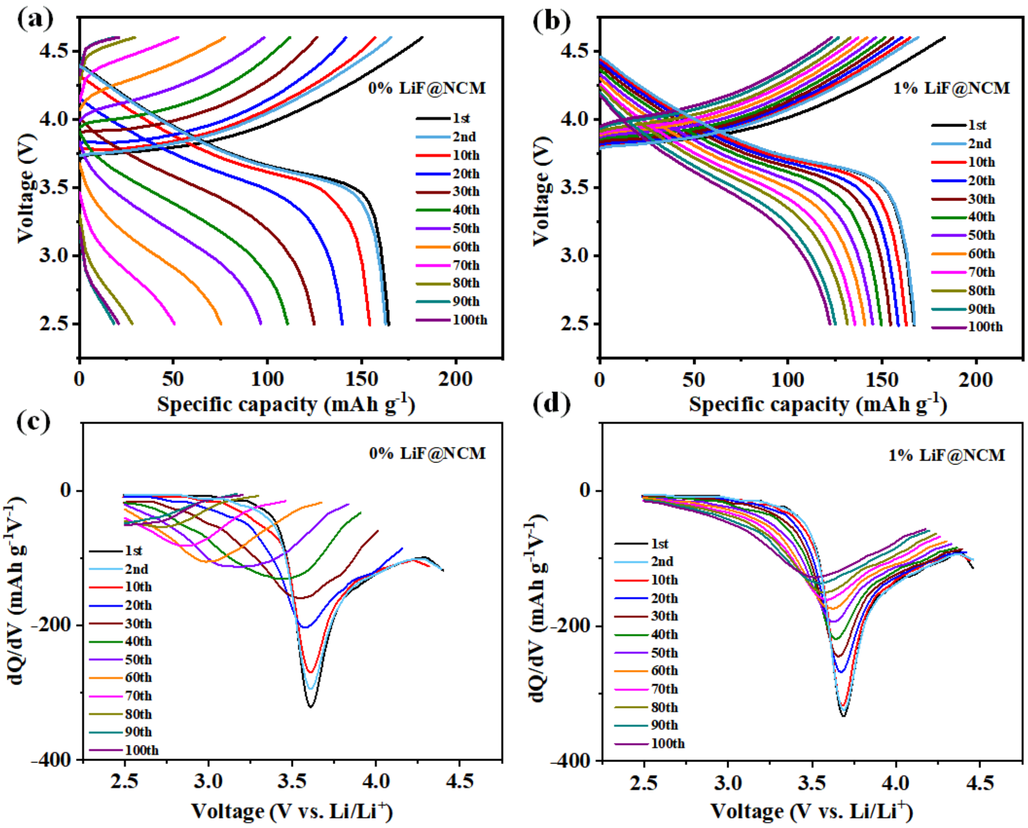

Figure 8. The electrochemical properties of (**a**) 0%LiF@NCM, (**b**) 1%LiF@NCM; dQ/dV curves of (**c**) 0%LiF@NCM, (**d**) 1%LiF@NCM.

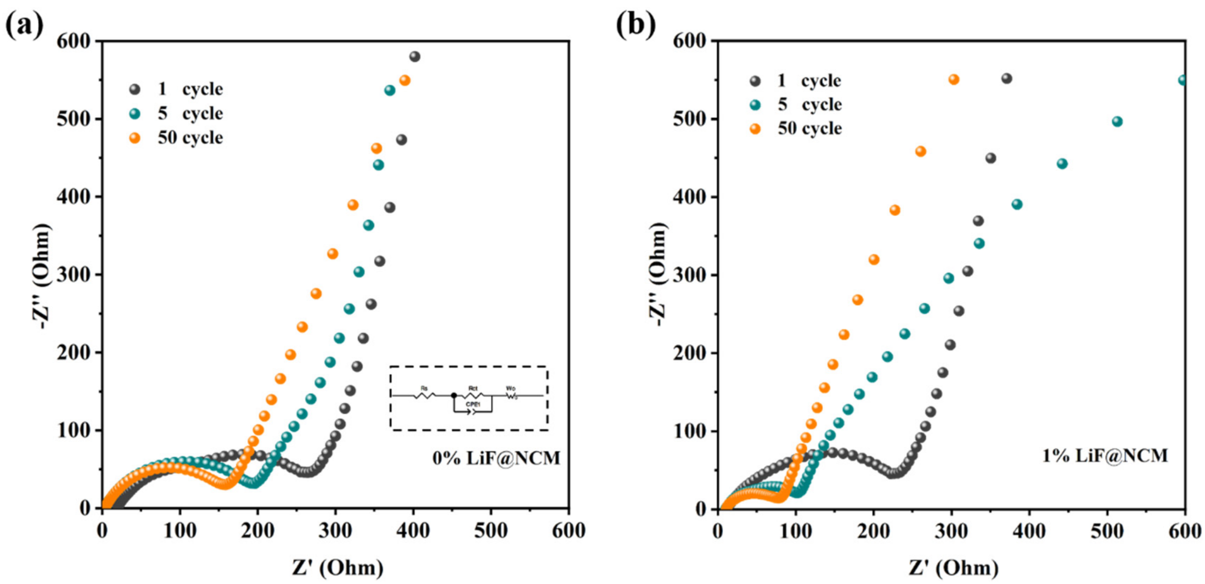

Figure 9. Nyquist plots of (**a**) 0%LiF@NCM and (**b**) 1%LiF@NCM electrodes after the 1st, 5th and 50th cycles (Inset shows the used equivalent circuit).

A comparison of the performance between our study and previous studies is shown in Table 1. It can be seen that the initial discharge capacity and the coulomb efficiency in our study is comparable to those reported in other literatures.

Table 1. The performances of our work compared to some previous reports.

Modification	Voltage Range (V)	Initial Specific Discharge Capacity (mAh g^{-1})	Coulombic Efficiency (%)	Test Conditions Specific Current (mA g^{-1})	Ref.
LiF	2.5–4.6	185	88.9	40	This work
$AlPO_4$	2.75–4.2	159	87.2	20	[41]
YPO_4	2.5–4.4	161.3	86.3	16	[42]
$Li_{1.3}Al_{0.3}Ti_{1.7}(PO_4)_3$/C	2.75–4.4	171	87.9	20	[13]
active carbon	2.5–4.5	191.2	91.1	85	[28]
fluoroborate glass	2.5–4.5	207.5	88.2	40	[11]
$LiTi_2(PO_4)_3$	2.8–4.5	191.5	91.1	85	[43]
lithium boron oxide	2.5–4.5	175.8	85.1	40	[44]
Al_2O_3	2.75–4.5	204.8	86.1	27.8	[45]
Li_2ZrO_3	3.0–4.6	197.8	86.0	16	[46]

4. Conclusions

In this work, a LiF surface layer is introduced on $LiNi_{1/3}Co_{1/3}Mn_{1/3}O_2$ via an in situ method. Results show the LiF modification can greatly improve the rate and cycling capabilities. Among them, the NCM sample treated with 1wt% LiF presents the best overall electrochemical performance, and it could reach a capacity retention of 83.4% after 100 cycles at 0.2C. EIS results suggest that the surface layer of the 1% LiF-modified sample is more stable than that of untreated NCM. Our results indicate that LiF surface modification is an effective method to enhance the electrochemical performance of NCM cathode materials, which may also be effective for other layered cathode materials.

Author Contributions: Formal analysis, Z.Z.; Investigation: S.L.; Writing—original draft preparation, S.Z.; Writing—review and supervision, R.W.; Project administration, X.Z. All authors have read and agreed to the published version of the manuscript.

Funding: This research was funded by Research on high power flexible battery in all sea depth (2020-XXXX-XX-246-00).

Institutional Review Board Statement: Not applicable.

Informed Consent Statement: Not applicable.

Data Availability Statement: All data that support the findings of this study are included within the article.

Conflicts of Interest: The authors declare no conflict of interest.

References

1. Goodenough, J.; Park, K. The Li-Ion Rechargeable Battery: A Perspective. *J. Am. Chem. Soc.* **2013**, *135*, 1167–1176. [CrossRef] [PubMed]
2. Wang, R.; Huang, B.; Qu, Z.; Gong, Y.; He, B.; Wang, H. Research on the kinetic properties of the cation disordered rock-salt Li-excess $Li_{1.25}Nb_{0.25}Mn_{0.5}O_2$ material. *Solid State Ion.* **2019**, *339*, 114999. [CrossRef]
3. Mauger, A.; Armand, M.; Julien, C.; Zaghib, K. Challenges and issues facing lithium metal for solid-state rechargeable batteries. *J. Power Sources* **2017**, *353*, 333–342. [CrossRef]
4. de Villers, B.T.; Bak, S.; Yang, J.; Han, S. In Situ ATR-FTIR Study of the Cathode–Electrolyte Interphase: Electrolyte Solution Structure, Transition Metal Redox, and Surface Layer Evolution. *Batter. Supercaps.* **2021**, *4*, 778–784. [CrossRef]
5. Yang, J.; Muhammad, S.; Jo, M.; Kim, H.; Song, K.; Agyeman, D.; Kim, Y.I.; Yoon, W.; Kang, Y. In situ analyses for ion storage materials. *Chem. Soc. Rev.* **2016**, *45*, 5717–5770. [CrossRef] [PubMed]
6. Yang, J.; Park, S.; Lee, S.; Kim, J.; Huang, D.; Gim, J.; Lee, E.; Kim, G.; Park, K.; Kang, Y.-M.; et al. High-voltage deprotonation of layered-type materials as a newly identified cause of electrode degradation. *J. Mater. Chem. A.* **2023**, *11*, 3018–3027. [CrossRef]
7. Manthiram, A.; Song, B.; Li, W. A perspective on nickel-rich layered oxide cathodes for lithium-ion batteries. *Energy Storage Mater.* **2017**, *6*, 125–139. [CrossRef]
8. Wang, R.; He, X.; He, L.; Wang, F.; Xiao, R.; Gu, L.; Li, H.; Chen, L. Atomic Structure of Li_2MnO_3 after Partial Delithiation and Re-Lithiation. *Adv. Energy Mater.* **2013**, *3*, 1358–1367. [CrossRef]

9. Xiong, X.; Wang, Z.; Yin, X.; Guo, H.; Li, X. A modified LiF coating process to enhance the electrochemical performance characteristics of $LiNi_{0.8}Co_{0.1}Mn_{0.1}O_2$ cathode materials. *Mater. Lett.* **2013**, *110*, 4–9. [CrossRef]
10. Ohzuku, T.; Makimura, Y. Layered lithium insertion material of $LiCo_{1/3}Ni_{1/3}Mn_{1/3}O_2$ for lithium-ion batteries. *Chem. Lett.* **2001**, *7*, 642–643. [CrossRef]
11. Zhang, Q.; Wang, L.; Zhu, C.; Sun, Z.; Cheng, W.; Lv, D.; Ren, W.; Bian, L.; Xu, J.; Chang, A. Enhanced Electrochemical Capability of $LiNi_{1/3}Co_{1/3}Mn_{1/3}O_2$ Cathode Materials Coated with Fluoroborate Glass for Lithium-Ion Batteries. *ChemElectroChem* **2017**, *4*, 1199–1204. [CrossRef]
12. Zhang, X.; Xiong, J.; Chang, F.; Xu, Z.; Wang, Z.; Hall, P.; Cheng, Y.; Xia, Y. Sol/Antisolvent Coating for High Initial Coulombic Efficiency and Ultra-stable Mechanical Integrity of Ni-Rich Cathode Materials. *ACS Appl. Mater. Interfaces* **2022**, *14*, 45272–45288. [CrossRef] [PubMed]
13. Yang, T.; Chin, C.-T.; Li, Y.; Cheng, C.-H. Sustainable Low-Temperature Coating of LATP/C Solid Electrolyte Composites on $LiNi_{1/3}Co_{1/3}Mn_{1/3}O_2$ Cathode Based on Lithium Iodide Solvent-Recrystallization for Li-Ion Batteries. *J. Electrochem. Soc.* **2022**, *169*, 113505. [CrossRef]
14. Li, G.; Feng, X.; Ding, Y.; Ye, S.; Gao, X. AlF_3-coated $Li(Li_{0.17}Ni_{0.25}Mn_{0.58})O_2$ as cathode material for Li-ion batteries. *Electrochim. Acta* **2012**, *78*, 308–315. [CrossRef]
15. Liu, X.; Liu, J.; Huang, T.; Yu, A. CaF_2-coated $Li_{1.2}Mn_{0.54}Ni_{0.13}Co_{0.13}O_2$ as cathode materials for Li-ionbatteries. *Electrochim. Acta* **2013**, *109*, 52–58. [CrossRef]
16. Chong, S.; Chen, Y.; Yan, W.; Guo, S.; Tan, Q.; Wu, Y.; Jiang, T.; Liu, Y. Suppressing capacity fading and voltage decay of Li-rich layered cathode material by a surface nano-protective layer of CoF_2 for lithium-ion batteries. *J. Power Sources* **2016**, *332*, 230–239. [CrossRef]
17. Zhang, X.; Belharouak, I.; Li, L.; Lei, Y.; Elam, J.W.; Nie, A.; Yassar, R.S.; Axelbaum, R.L. Structural and Electrochemical Study of Al_2O_3 and TiO_2 coated $Li_{1.2}Ni_{0.13}Mn_{0.54}Co_{0.13}O_2$ Cathode Material Using ALD. *Adv. Energy Mater.* **2013**, *3*, 1299–1307. [CrossRef]
18. Huang, B.; Wang, R.; Gong, Y.; He, B.; Wang, H. Enhanced Cycling Stability of Cation Disordered Rock-Salt $Li_{1.2}Ti_{0.4}Mn_{0.4}O_2$ Material by Surface Modification With Al_2O_3. *Front. Chem.* **2019**, *7*, 107. [CrossRef]
19. Chen, D.; Zheng, F.; Li, L.; Chen, M.; Zhong, X.; Li, W.; Lu, L. Effect of Li_3PO_4 coating of layered lithium-rich oxide on electrochemical performance. *J. Power Sources* **2017**, *341*, 147–155. [CrossRef]
20. Wu, F.; Zhang, X.; Zhao, T.; Li, L.; Xie, M.; Chen, R. Multifunctional $AlPO_4$ coating for improving electrochemical properties of low-cost $Li[Li_{0.2}Fe_{0.1}Ni_{0.15}Mn_{0.55}]O_2$ cathode materials for lithium-ion batteries. *ACS Appl. Mater. Interfaces* **2015**, *7*, 3773–3781. [CrossRef]
21. Wang, Z.; Liu, E.; He, C.; Shi, C.; Li, J.; Zhao, N. Effect of amorphous $FePO_4$ coating on structure and electrochemical performance of $Li_{1.2}Ni_{0.13}Co_{0.13}Mn_{0.54}O_2$ as cathode material for Li-ion batteries. *J. Power Sources* **2013**, *236*, 25–32. [CrossRef]
22. Zhang, M. Enhanced Electrochemical Performance of $LiNi_{1/3}Co_{1/3}Mn_{1/3}O_2$ at a High Cut-Off Voltage of 4.6 V by $Li_{1.3}Al_{0.3}Ti_{1.7}(PO_4)_3$ Coating. *Coatings* **2022**, *12*, 1964. [CrossRef]
23. Qu, Z.; Liu, S.; Zhang, P.; Wang, R.; Wang, H.; He, B.; Gong, Y.; Jin, J.; Li, S. Enhanced eletrochemical performances of $LiCoO_2$ at high cut-off voltage by introducing LiF additive. *Solid State Ion.* **2021**, *365*, 115654. [CrossRef]
24. Yu, K.; Chen, J.; Lin, K.; Li, J.; Shi, Z. Constructing LiF-rich artificial SEI at a two-dimensional copper net current collector in anode-free lithium metal batteries. *Surf. Interfaces* **2022**, *34*, 102326. [CrossRef]
25. Liu, K.; Zhang, Q.; Dai, S.; Li, W.; Liu, X.; Ding, F.; Zhang, J. Effect of F^- doping and LiF coating on improving the high-voltage cycling stability and rate capacity of $LiNi_{0.5}Co_{0.2}Mn_{0.3}O_2$ cathode materials for lithium-ion batteries. *ACS Appl. Mater. Interfaces* **2018**, *10*, 34153. [CrossRef] [PubMed]
26. Ding, X.; Li, Y.; Chen, F.; He, X.; Yasmin, A.; Hu, Q.; Wen, Z.; Chen, C. In situ formation of LiF decoration on a Li-rich material for long-cycle life and superb low-temperature performance. *J. Mater. Chem. A* **2019**, *7*, 11513–11519. [CrossRef]
27. Fu, C.; Wang, J.; Wang, J.; Meng, L.; Zhang, W.; Li, X.; Li, L. A $LiPF_6$-electrolyte-solvothermal route for the synthesis of $LiF/Li_xPF_yO_z$-coated Li-rich cathode materials with enhanced cycling stability. *J. Mater. Chem. A* **2019**, *7*, 23149–23161. [CrossRef]
28. Yang, C.; Zhang, X.; Huang, M.; Huang, J.; Fang, Z. Preparation and Rate Capability of Carbon Coated $LiNi_{1/3}Co_{1/3}Mn_{1/3}O_2$ as Cathode Material in Lithium Ion Batteries. *ACS Appl. Mater. Interfaces* **2017**, *9*, 12408–12415. [CrossRef]
29. Deng, R.; Tao, J.; Zhong, W.; Wen, L.; Yang, Y.; Li, J.; Lin, Y. Tri-functionalized $Li_2B_4O_7$ coated $LiNi_{0.5}Co_{0.2}Mn_{0.3}O_2$ for boosted performance lithium-ion batteries. *J. Alloys Compd.* **2023**, *940*, 168767. [CrossRef]
30. Zhuang, Y.; Zhao, Y.; Bao, Y.; Zhang, W.; Guan, M. Research on the electrochemical properties of vanadium boride coated on the surface of NCM811. *J. Alloys Compd.* **2022**, *927*, 166967. [CrossRef]
31. Dunlap, N.; Sulas-Kern, D.; Weddle, P.; Usseglio-Viretta, F.; Walker, P.; Todd, P.; Boone, D.; Colclasure, A.; Smith, K.; de Villers, B.T.; et al. Laser ablation of Li-ion electrodes for fast charging: Material properties, rate capability, Li plating, and wetting. *J. Power Sour.* **2022**, *537*, 231464. [CrossRef]
32. Yi, H.; Tan, L.; Xia, L.; Li, L.; Li, H.; Liu, Z.; Wang, C.; Zhao, Z.; Duan, J.; Chen, Z. Ce-modified $LiNi_{0.5}Co_{0.2}Mn_{0.3}O_2$ cathode with enhanced surface and structural stability for Li ion batteries. *Adv. Powder Technol.* **2021**, *32*, 2493–2501. [CrossRef]
33. Ma, S.; Zhang, X.; Li, S.; Cui, Y.; Cui, Y.; Zhao, Y.; Cui, Y. In situ formed $LiNi_{0.8}Co_{0.1}Mn_{0.1}O_2$@LiF composite cathode material with high rate capability and long cycling stability for lithium-ion batteries. *Ionics* **2020**, *26*, 2165–2176. [CrossRef]

34. Zhang, Y.; Self, E.; Thapaliya, B.; Giovine, R.; Meyer, H.; Li, L.; Yue, Y.; Chen, D.; Tong, W.; Chen, G.; et al. Formation of LiF Surface Layer during Direct Fluorination of High-Capacity Co-Free Disordered Rocksalt Cathodes. *ACS Appl. Mater. Interfaces* **2021**, *13*, 38221–38228. [CrossRef]
35. Liu, Y.; Fan, X.; Huang, X.; Liu, D.; Dou, A.; Su, M.; Chu, D. Electrochemical performance of $Li_{1.2}Ni_{0.2}Mn_{0.6}O_2$ coated with a facilely synthesized $Li_{1.3}Al_{0.3}Ti_{1.7}(PO_4)_3$. *J. Power Sources* **2018**, *403*, 27–37. [CrossRef]
36. Xue, L.; Li, Y.; Xu, B.; Chen, Y.; Cao, G.; Li, J.; Deng, S.; Chen, Y.; Chen, J. Effect of Mo doping on the structure and electrochemical performances of $LiNi_{0.6}Co_{0.2}Mn_{0.2}O_2$ cathode material at high cut-off voltage. *J. Alloys Compd.* **2018**, *748*, 561–568. [CrossRef]
37. Wang, H.; Hashem, A.; Abdel-Ghany, A.; Abbas, S.; El-Tawil, R.; Li, T.; Li, X.; El-Mounayri, H.; Tovar, A.; Zhu, L.; et al. Effect of Cationic (Na^+) and Anionic (F^-) Co-Doping on the Structural and Electrochemical Properties of $LiNi_{1/3}Mn_{1/3}Co_{1/3}O_2$ Cathode Material for Lithium-Ion Batteries. *Int. J. Mol. Sci.* **2022**, *23*, 6755. [CrossRef] [PubMed]
38. Wang, R.; Li, X.; Liu, L.; Lee, J.; Seo, D.-H.; Bo, S.-H.; Urban, A.; Ceder, G. A disordered rock-salt Li-excess cathode material with high capacity and substantial oxygen redox activity: $Li_{1.25}Nb_{0.25}Mn_{0.5}O_2$. *Electrochem. Commun.* **2015**, *60*, 70–73. [CrossRef]
39. Zhang, X.; Sui, X.; Zhou, S.; Tang, C.; Wang, R. Li-B alloy with artificial solid electrolyte interphase layer for long-life lithium metal batteries. *Solid State Ion.* **2020**, *354*, 115408. [CrossRef]
40. Kasnatscheew, J.; Evertz, M.; Streipert, B.; Wagner, R.; Klöpsch, R.; Vortmann, B.; Hahn, H.; Nowak, S.; Amereller, M.; Gentschev, A.; et al. The truth about the 1st cycle Coulombic efficiency of $LiNi_{1/3}Co_{1/3}Mn_{1/3}O_2$ (NCM) cathodes. *Phys. Chem. Chem. Phys.* **2016**, *18*, 3956–3965.24. [CrossRef]
41. Wang, J.; Wang, Y.; Guo, Y.; Liu, C.; Dan, L. Electrochemical characterization of AlPO4 coated $LiNi_{1/3}Co_{1/3}Mn_{1/3}O_2$ cathode materials for high temperature lithium battery application. *Rare Met.* **2021**, *40*, 78. [CrossRef]
42. Bai, Y.; Chang, Q.; Yu, Q.; Zhao, S.; Jiang, K. A novel approach to improve the electrochemical performances of layered $LiNi_{1/3}Co_{1/3}Mn_{1/3}O_2$ cathode by YPO_4 surface coating. *Electrochim. Acta* **2013**, *112*, 414. [CrossRef]
43. Zhang, L.-L.; Wang, J.-Q.; Yang, X.-L.; Liang, G.; Li, T.; Yu, P.-L.; Ma, D. Enhanced Electrochemical Performance of Fast Ionic Conductor $LiTi_2(PO_4)_3$-Coated $LiNi_{1/3}Co_{1/3}Mn_{1/3}O_2$ Cathode Material. *ACS Appl. Mater. Interfaces* **2018**, *10*, 11663. [CrossRef] [PubMed]
44. Tan, S.; Wang, L.; Bian, L.; Xu, J.; Ren, W.; Hu, P.; Chang, A. Highly enhanced low temperature discharge capacity of $LiNi_{1/3}Co_{1/3}Mn_{1/3}O_2$ with lithium boron oxide glass modification. *J. Power Sources* **2015**, *277*, 139. [CrossRef]
45. Shen, D.; Zhang, D.; Wen, J.; Chen, D.; He, X.; Yao, Y.; Li, X.; Duger, C. $LiNi_{1/3}Co_{1/3}Mn_{1/3}O_2$ coated by Al_2O_3 from urea homogeneous precipitation method: Improved Li storage performance and mechanism exploring. *J. Solid State Electrochem.* **2015**, *19*, 1523. [CrossRef]
46. Wang, W.; Yin, Z.; Wang, J.; Wang, Z.; Li, X.; Guo, H. Effect of heat-treatment on Li_2ZrO_3-coated $LiNi_{1/3}Co_{1/3}Mn_{1/3}O_2$ and its high voltage electrochemical performance. *J. Alloys Compd.* **2015**, *651*, 737. [CrossRef]